Modifications of the quasi-biennial oscillation by a geoengineering perturbation of the stratospheric aerosol layer

V. Aquila[1,2], C. I. Garfinkel[3], P.A. Newman[4], L.D. Oman[4], D.W. Waugh[2]

[1] Goddard Earth Science Technology & Research (GESTAR)

[2] Department of Earth and Planetary Sciences, Johns Hopkins University, Baltimore, MD

[3] The Fredy & Nadine Herrmann Institute of Earth Sciences, Hebrew University, Jerusalem, Israel

[4] NASA Goddard Space Flight Center, Greenbelt, MD

This article has been accepted for publication and undergone full peer review but has not been through the copyediting, typesetting, pagination and proofreading process which may lead to differences between this version and the Version of Record. Please cite this article as doi: 10.1002/2013GL058818

Abstract

This paper examines the impact of geoengineering via stratospheric sulfate aerosol on the quasi-biennial oscillation (QBO) using the NASA Goddard Earth Observing System (GEOS-5) Chemistry Climate Model. We performed four 30-year simulations with a continuous injection of sulfur dioxide on the equator at 0˚ longitude. The four simulations differ by the amount of sulfur dioxide injected (5Tg/year and 2.5 Tg/year) and the altitude of the injection (16km-25km and 22km-25km). We find that such an injection dramatically alters the quasi-biennial oscillation, prolonging the phase of easterly shear with respect to the control simulation. This is caused by the increased aerosol heating, and associated warming in the tropical lower stratosphere and higher residual vertical velocity. In the case of maximum perturbation, *i.e.* highest stratospheric aerosol burden, the lower tropical stratosphere is locked into a permanent westerly QBO phase.

Introduction

The quasi-biennial oscillation (QBO) is an approximately 28-month period oscillation of zonally symmetric easterly and westerly winds in the tropical stratosphere. The QBO is caused by vertically propagating waves, such as equatorial Kelvin and Rossby-gravity waves, that deposit momentum in the stratosphere [e.g. *Baldwin et al.*, 2001]. While the QBO is confined to the tropics, its phase affects the stratospheric transport to the extratropics and the strength of the polar vortex [*Holton and Tan*, 1980], altering transport from the tropics to mid- and high latitudes of stratospheric trace gases and aerosols [*Trepte and Hitchman,* 1992]. Additionally, studies have shown that the QBO can impact the tropospheric winds (*Garfinkel and Hartmann,* 2011) and precipitation (*Jihoon et al.* 2013).

The vertical descent of the QBO wind shear is linked to the mean tropical upwelling of the Brewer-Dobson circulation (BDC) [*e.g. Watanabe and Kawatani*, 2012]. *Kawatani and Hamilton* (2013) identified in radiosonde observations for the 1953-2012 period a long-term trend of weakening QBO amplitude, which they attributed to the BDC strengthening due to increasing greenhouse gases.

Geoengineering is a deliberate modification of the Earth system in order to counteract global warming due to increasing greenhouse gases. Some proposed geoengineering methods address the causes of the warming by reducing the amount of solar radiation reaching the Earth surface (solar radiation management or SRM), for instance by continuously injecting sulfate aerosol into the stratosphere. This method aims to reproduce the global surface cooling observed after major volcanic eruptions.

In addition to its effect on tropospheric temperatures (*Kravitz et al.,* 2013), precipitation (*Haywood et al.,* 2013; *Tilmes et al.,* 2013) and stratospheric ozone (*Tilmes et al.,* 2009), such stratospheric injection of aerosol would also lead to perturbations of stratospheric dynamics. An increase in stratospheric aerosol loading would warm the lower stratosphere, mainly via absorption of longwave radiation. Such warming would lead to a strengthening of the tropical upwelling, as showed by *Aquila et al.* (2012) in the case of a Mt. Pinatubo-like eruption, which could interfere with the periodicity of the QBO. After the Mt. Pinatubo eruption, observations showed a warming of the lower stratosphere of about 3K, and a delay in the downward propagation of the easterly shear [*Labitzke*, 1993].

Here, we present a set of four model experiments that simulate the geoengineering stratospheric injection of sulfur dioxide, varying the burden and altitude of the SO_2 injection, in order to investigate the impact of stratospheric aerosol geoengineering on the QBO.

Model simulations

The Goddard Earth Observing System Chemistry Climate Model (GEOSCCM) couples the GEOS-5 general circulation model [*Rienecker et al.*, 2011], the Georgia Institute of Technology-Goddard Global Ozone Chemistry Aerosol Radiation and Transport (GOCART) module [*Colarco et al.*, 2010] and the StratChem stratospheric chemistry module [*Pawson et al.,* 2008]. GOCART is a bulk aerosol model which include a parameterization of the chemical production of SO_4 aerosol from oxidation of dimethyl sulfide (DMS) by OH during day and NO_3 during night, and from oxidation of SO_2 by OH in the gas phase and by H_2O_2 in the aqueous phase. Evaluation of a similar version of GEOSCCM with

respect to stratospheric aerosol by *Aquila et al.* [2012; 2013] shows good agreement with observations of aerosol distributions and ozone and NO_2 depletion after the eruption of Mount Pinatubo. Compared to *Aquila et al.* (2013), this GEOSCCM version includes both a mechanism to generate the QBO using a gravity wave drag parameterization [*Molod et al.*, 2012], and a coupling between aerosol and heterogeneous chemistry via the aerosol surface area density. The aerosol surface area density is calculated from the dry sulfate mass assuming that the aerosol particles are lognormally distributed with modal radius 0.35 μm. This same size distribution, hydrated accordingly to the relative humidity, is used to calculate the optical properties of the stratospheric sulfate aerosol and its settling velocity.

The GEOSCCM resolution is 2.0° latitude by 2.5° longitude, with 72 vertical hybrid levels from surface to 0.01 hPa. The model is prescribed with sea surface temperatures and sea ice concentrations calculated with the Community Earth System Model (CESM) [*Gent et al.*, 2011] using emission inventories valid for the Representative Concentration Pathway (RCP) 4.5 [*Taylor et al.*, 2012].

We performed four 30-year long experiments from 2020 to 2049 in which we prescribed a continuous injection of SO_2 in the stratosphere on the equator at 0° longitude. The four perturbed simulations differ from each other with regard to the burden (5 Tg/year in two of the experiments and 2.5 Tg/year in the other two) and altitude (16km-25km and 22km-25km) of the geoengineering injection. The four experiments ($G_5^{16\text{-}25km}$, $G_{2.5}^{16\text{-}25km}$, $G_5^{22\text{-}25km}$ and $G_{2.5}^{22\text{-}25km}$) are summarized in Table 1. $G_5^{16\text{-}25km}$ corresponds to the experiment G4 of the Geoengineering Model Intercomparison Project (GeoMIP; *Kravitz et al.*, 2011).

Additionally, we performed a control simulation without stratospheric SO_2 injection.

We concentrate in our discussion on the last 20 years of simulations, when the sources and sinks of geoengineering aerosol are in equilibrium. During this time span, the atmospheric burden of the geoengineering sulfate aerosol is equal to 4.7 Tg-S in $G_5^{22\text{-}25km}$, 3.1 Tg-S in $G_5^{16\text{-}25km}$, 2.1 Tg-S in $G_{2.5}^{22\text{-}25km}$ and 1.5 Tg-S in $G_{2.5}^{16\text{-}25km}$ (Table 1). The mixing between the tropics and extra-tropics is weaker at the altitudes where the aerosol is injected in $G_5^{22\text{-}25km}$ and $G_{2.5}^{22\text{-}25km}$ than at lower altitudes (16-20 km), and this leads to longer stratospheric residence times and higher aerosol burdens in these experiments (Table 1). For comparison, *Baran and Foot* (1994) measured a maximum stratospheric aerosol burden of about 7 Tg-S after the eruption of Mt. Pinatubo, which decreased to 4 Tg-S about 18 months after the eruption. The vertical distribution of the geoengineering aerosol in the four simulations is shown in Fig. 1 of the supplementary material. The total burden in our simulations are similar to that in the geoengineering experiments of Heckendorn et al. (2009), but the aerosols are more confined to the tropics in our simulations. This is likely due to differences in the transport (Heckendorn et al. (2009) use a two-dimensional model), but could also be due to differences in the injection height and microphysical processes.

The stratospheric aerosol optical thickness (AOT) can be roughly converted to radiative forcing by multiplying by 25 W/m^2 (*Hansen et al.*, 2005). Using this conversion factor, the aerosol radiative forcing in our simulations ranges from -1Wm^{-2} in $G_{2.5}^{16\text{-}25km}$ to -3 Wm^{-2} in $G_5^{22\text{-}25km}$ (see Fig. 2 supplementary material for the simulated AOT). Even in a fairly optimistic scenario such as the

Representative Concentration Pathways (RCP) 4.5 [*Clarke et al.*, 2007; *Smith et al.*, 2006; *Wise et al.,* 2009], the radiative forcing by increasing greenhouse gases reaches $3Wm^{-2}$ around 2030. Hence, the aerosol perturbations introduced in our experiments are within the possible range that might be needed to offset warming from increasing greenhouse gases.

Note that in these experiments, the source function for gravity waves is held fixed in all experiments and is not coupled to convection, and the sea surface temperatures (SSTs) do not vary among the experiments. It is likely that the SSTs and the convection will change were geo-engineering implemented. Hence, the source of wave driving for the QBO in these experiments does not vary realistically in response to geo-engineering, and future work is necessary to explore whether these limitations affect the model results presented below.

Results

Our results show that the stratospheric aerosol injection dramatically perturbs the QBO periodicity, prolonging the phase of easterly shear with respect to the control case. Figure 1 shows the vertical profiles of the tropical zonal wind, averaged between 2˚S and 2˚N, in the control simulation (upper panel) and in the four geoengineering experiments. The phase of easterly shear persists for longer and longer with increasing stratospheric burden of aerosol. Table 1 reports the mean value and standard deviation of the simulated QBO period: the period of the QBO increases with the burden of geoengineering aerosol, from about 25 months in the control simulation to about 50 months in $G_5^{16\text{-}25km}$. The QBO completely disappears in $G_5^{22\text{-}25km}$ (lowest panel), where the stratosphere is in a perpetual easterly shear or westerly phase. In the following discussion we will focus on $G_5^{22\text{-}25km}$. The response of the QBO to the increase of aerosol is fast,

within one QBO period in the G_5 experiments, and within two QBO periods in $G_{2.5}$. Additionally, between 17 km and 30 km altitude the amplitude of the QBO decreases with increasing stratospheric aerosol burden (Fig. 3 of supplementary material).

Figure 2 shows the mechanism that leads to the interruption of the QBO in $G_5^{22\text{-}25\text{km}}$. The heating from the geoengineering aerosol induces a warming of the lower stratosphere up to about 27 km altitude (Fig. 2, upper left panel). Because the radiative damping timescales are longer in the lower stratosphere than in the upper stratosphere, the aerosols affect lower stratospheric temperature more strongly (Newman and Rosenfield, 1997). The warmer temperature centered on the equator induces an equatorial positive wind shear ($\beta\bar{u}_z = -R\bar{T}_{yy}/H$), which results in persistent westerly winds between 20 and 30 km. The heating anomaly due to the aerosol also causes an increase of the residual vertical velocity $\bar{w}^*$ (Fig. 2, upper right panel), which advects the aerosol upward from the initial injection altitude. The increase in $\bar{w}^*$ extends well above the level at which the diabatic heating ends, consistent with *Holloway and Neelin* (2007) and *Garfinkel et al.* (2013).

The typical processes that lead to the QBO's downward propagation weaken in the presence of the increase to $\bar{w}^*$due to the geoengineering aerosols. This effect is demonstrated by the lower panels of Fig. 2, which show the budget of the terms that force the QBO in the control and $G_5^{22\text{-}25\text{km}}$ experiments, averaged between 2°S and 2°N. When the QBO propagates downwards, momentum deposition from the parameterized gravity waves (GWD) drives the downward propagation, but it is opposed (but not fully) by westerly momentum from the vertical advection of the mean flow ($-\bar{w}^*\bar{u}_z$)which advects the wind anomalies

upwards. In the presence of aerosols and enhanced $\bar{w}^*$, the easterly momentum from the parameterized gravity waves (GWD) and the westerly momentum from the vertical advection of the mean flow ($-\bar{w}^*\bar{u}_z$) balance each other leading to a smaller time derivative of the zonal wind.

Figure 3 shows the anomalies of temperature, zonal winds, and ozone and N_2O concentrations in $G_5^{22\text{-}25km}$ with respect to the control simulation. The circulation anomaly is also superimposed on Fig. 3. The temperature anomalies (Fig. 3, upper left) shows the largest warming centered at about 20 km and related to the absorption of longwave radiation by the aerosol. The cold anomaly above this region near 30km is related to the circulation anomaly caused by the aerosol. This induced circulation is also clearly reflected in the N_2O concentrations (Fig. 3, lower right). N_2O is a well-suited tracer to study stratospheric transport, due to its long stratospheric lifetime and its distribution with higher concentrations at the surface in the tropics. The circulation changes induced by the aerosol increase the N_2O concentrations in the middle stratosphere and enhance its transport to the extratropics. The ozone anomalies (Fig. 3, lower left) are due to a combination of heterogeneous chemistry on the aerosol particles and to the induced change in tropical dynamics (*Aquila et al.* 2013), which advects air with different ozone concentrations. Similar changes are also found in the other simulations (see supplementary material); there are some differences in the spatial structure of the anomalies among the experiments, and future work is needed to examine these differences

Conclusions

Our simulations show that geoengineering injection of stratospheric aerosol can lead to dramatic changes in the QBO, prolonging the phase of easterly shear with

respect to the control simulation. For very large increases in stratospheric aerosol burden (4.7 Tg-S), the lower tropical stratosphere is locked into a permanent westerly QBO phase. Fig. 7 in the supplementary material suggests that there is roughly a quadratic relationship between the aerosol burden and the QBO period, calculated at 30 hPa. This modification of the QBO occurs because the increase in aerosol burden leads to a warming of the tropical lower-middle stratosphere, mainly via absorption of longwave radiation, and, hence, to stronger westerly winds resulting from the thermal wind relation. This warming also induces an increase in the residual vertical velocity $\bar{w}^*$, which broadens the band of westerly winds and lofts the aerosol higher in the stratosphere. Because the QBO can impact stratospheric and tropospheric ozone (*Randel and Wu*, 1996; *Ziemke and Chandra*, 1999; *Oman et al*., 2013), tropospheric winds (*Garfinkel and Hartmann,* 2011), and precipitation (*Jihoon et al.* 2013), this geoengineering-forced permanent lower stratospheric QBO westerly phase could substantially alter surface climate.

References

Aquila, V., L. D. Oman, R. S. Stolarski, P. R. Colarco, and P. A. Newman (2012), Dispersion of the volcanic sulfate cloud from a Mount Pinatubo–like eruption, *J. Geophys. Res., 117*, D06216. doi:10.1029/2011JD016968.

Aquila, V., L. D. Oman, R. Stolarski, A. R. Douglass, and P. A. Newman (2013), The Response of Ozone and Nitrogen Dioxide to the Eruption of Mt. Pinatubo at Southern and Northern Midlatitudes*, J. Atmos. Sci., 70(3)*, 894–900. doi:10.1175/JAS-D-12-0143.1.

Baldwin, M. P., Gray, L. J., Dunkerton, T. J., Hamilton, K., Haynes, P. H., Randel, et al. (2001). The quasi-biennial oscillation. *Rev. Geophys*., 179–229. doi: 8755-1209/01/1999RG000073

Baran, A. J., & Foot, J. S. (1994). New application of the operational sounder HIRS in determining climatology of sulphuric acid aerosol from the Pinatubo eruption. *J. Geophys. Res.*, *99*(D12), 25673–25679. doi:10.1029/94JD02044

Clarke, L., J. Edmonds, H. Jacoby, H. Pitcher, J. Reilly, R. Richels, 2007. Scenarios of Greenhouse Gas Emissions and Atmospheric Concentrations. Sub-report 2.1A of Synthesis and Assessment Product 2.1 by the U.S. Climate Change Science Program and the Subcommittee on Global Change Research. Department of Energy, Office of Biological & Environmental Research, Washington, 7 DC., USA, 154 pp.

Colarco, P., A. Da Silva, M. Chin, and T. Diehl (2010), Online simulations of global aerosol distributions in the NASA GEOS-4 model and comparisons to satellite and ground-based aerosol optical depth, *J. Geophys. Res.*, *115(D14)*, D14207. doi:10.1029/2009JD012820.

Garfinkel, C. I., and D. L. Hartmann (2011), The influence of the quasi-biennial oscillation on the troposphere in winter in a hierarchy of models. Part I: Simplified dry GCM runs, *J. Atmos. Sci.*, *68*, 1273–1289.

Garfinkel, C.I., D. W. Waugh, L.D. Oman, L. Wang, and M.M. Hurwitz, (2013). Temperature trends in the tropical upper troposphere and lower stratosphere: connections with sea surface temperatures and implications for water vapor and ozone, *J. Geophys. Res.*, 118(17), 9658-9672, doi: 10.1002/jgrd.50772.

Gent, P. R., G. Danabasoglu, L. J. Donner, M. M. Holland, E. C. Hunke, S. R. Jayne, D. M. Lawrence, et al. (2011), The Community Climate System Model Version 4, *J. Clim., 24(19)*, pp. 4973–4991, doi: 10.1175/2011JCLI4083.

Hansen, J., Sato, M., Ruedy, R., Nazarenko, L., Lacis, A., Schmidt, G., et al. (2005). Efficacy of climate forcings. *J. Geophys. Res.*, *110*(D18), D18104. doi:10.1029/2005JD005776

Haywood, J. M., A. Jones, N. Bellouin, and D. Stephenson (2013), Asymmetric forcing from stratospheric aerosols impacts Sahelian rainfall, *Nature Climate Change*, *3*, 660-665, doi:10.1038/nclimate1857.

Heckendorn, P., D. Weisenstein, S. Fueglistaler, B. P. Luo, E. Rozanov, M. Schraner, L. W. Thomason, and T. Peter. The impact of geoengineering aerosols on stratospheric temperature and ozone. *Environmental Research Letters* 4, no. 4 (2009): 045108.

Holloway, C. E., & Neelin, J. D. (2007). The Convective Cold Top and Quasi Equilibrium. *J. Atmos. Sci. 64*(5), 1467–1487. doi:10.1175/JAS3907.1

Holton, J. R. and H. C. Tan (1980). The influence of the equatorial quasi-biennial oscillation on the global circulation at 50 mb. *J. Atmos. Sci.*, 37, 2200–2208.

Jihoon, S., Choi, W., Youn, D., Park, D.-S. R., & Kim, J. Y. (2013). Relationship between the stratospheric quasi-biennial oscillation and spring rainfall in the western North Pacific. *Geophys. Res. Lett.*,in press. doi:10.1002/2013GL058266

Kawatani, Y., & Hamilton, K. (2013). Weakened stratospheric quasibiennial oscillation driven by increased tropical mean upwelling. *Nature*, *497*(7450), 478–481. doi:10.1038/nature12140

Kravitz, B., Robock, A., Boucher, O., Schmidt, H., Taylor, K. E., Stenchikov, G., and Schulz, M. (2011). The Geoengineering Model Intercomparison Project (GeoMIP). *Atmos. Sci. Let.*, *12*(2), 162–167. doi:10.1002/asl.316

Kravitz, B., Caldeira, K., Boucher, O., Robock, A., Rasch, P. J., Alterskjaer, K., Karam, D. B., et al., (2013). Climate model response from the Geoengineering Model Intercomparison Project (GeoMIP). *J. Geophys. Res.*, *118*, 1–13. doi:10.1002/jgrd.50646

Labitzke, K., (1994). Stratospheric temperature changes after the Pinatubo eruption. *J. Atmos. Terr. Phys.,* 56(9), 1027-1034. doi:10.1016/0021-9169(94)90039-6

Molod, A., L. Takacs, M. Suarez, J. Bacmeister, I.-S. Song, and A. Eichmann (2012), The GEOS-5 Atmospheric General Circulation Model: Mean Climate and Development from MERRA to Fortuna. Technical Report Series on Global Modeling and Data Assimilation, 28.

Newman, P. A., and Rosenfield, J. E. (1997). Stratospheric thermal damping times. *Geophysical research letters*, *24*(4), 433-436, DOI: 10.1029/96GL03720.

Oman, L. D., A. R. Douglass, J. R. Ziemke, J. M. Rodriguez, D. W. Waugh, and J. E. Nielsen, 2013: The ozone response to ENSO in Aura satellite measurements and a chemistry-climate simulation, J. Geophys. Res., 118, 965-976, doi:10.1029/2012JD018546

Pawson, S., R. S. Stolarski, A. R. Douglass, P. A. Newman, J. E. Nielsen, S. M. Frith, and M. L. Gupta (2008), Goddard Earth Observing System chemistry-climate model simulations of stratospheric ozone-temperature coupling between 1950 and 2005, *J. Geophys. Res., 113(D12)*, D12103. doi:10.1029/2007JD009511.

Randel, W. J., and Wu, F. (1996), Isolation of the ozone QBO in SAGE II data by singular-value decomposition. *Journal of the atmospheric sciences*, *53*(17), 2546-2559.

Rienecker, M. M., M. J. Suarez, R. Gelaro, R. Todling, J. Bacmeister, E. Liu, et al. (2011), MERRA: NASA's Modern-Era Retrospective Analysis for Research and Applications, *J. Clim., 24(14)*, 3624–3648. doi:10.1175/JCLI-D-11-00015.1.

Smith, S.J. and T.M.L. Wigley, 2006. Multi-Gas Forcing Stabilization with the MiniCAM. Energy Journal (Special Issue #3) pp 373-391.

Taylor, K. E., R. J. Stouffer, and G. A. Meehl (2012), An Overview of CMIP5 and the Experiment Design, *Bull. Amer. Meteor. Soc*., 93, 485–498. doi:10.1175/BAMS-D-11-00094.1

Tie, X., & Brasseur, G. (1995). The response of stratospheric ozone to volcanic eruptions: Sensitivity to atmospheric chlorine loading. *Geophys. Res. Lett.*, *22*(22), 3035–3038. doi:10.1029/95GL03057

Tilmes, S., Garcia, R. R., Kinnison, D. E., Gettelman, A., & Rasch, P. J. (2009). Impact of geoengineered aerosols on the troposphere and stratosphere. *J. Geophys. Res.*, *114*(D12). doi:10.1029/2008JD011420

Tilmes, S., Garcia, R. R., Kinnison, D. E., Gettelman, A., & Rasch, P. J. (2009). Impact of geoengineered aerosols on the troposphere and stratosphere. *J. Geophys. Res.*, *114*(D12). doi:10.1029/2008JD011420

Tilmes, S., J. Fasullo, J.-F. Lamarque, D. R. Marsch, M. Mills, K. Alterskjær, et al. (2013), The hydrological impact of geoengineering in the Geoengineering Model Intercomparison Project (GeoMIP), *J. Geophys. Res.,* 118(19),11036-11058. doi: 10.1002/jgra.50868.

Trepte, C. R., & Hitchman, M. H. (1992). Tropical stratospheric circulation deduced from satellite aerosol data. *Nature*, *335*, 626–628. doi:10.1038/355626a0

Watanabe, S., & Kawatani, Y. (2012). Sensitivity of the QBO to Mean Tropical Upwelling under a Changing Climate Simulated with an Earth System Model. *J. Meteorol. Soc. Jpn.*, *90A*(0), 351–360. doi:10.2151/jmsj.2012-A20

Wise, MA, KV Calvin, AM Thomson, LE Clarke, B Bond-Lamberty, RD Sands, SJ Smith, AC Janetos, JA Edmonds. 2009. Implications of Limiting CO2 Concentrations for Land Use and Energy. Science. 324:1183-1186. May 29, 2009.

Ziemke, J. R., and Chandra, S. (1999). Seasonal and interannual variabilities in tropical tropospheric ozone. *Journal of Geophysical Research: Atmospheres (1984–2012)*, *104*(D17), 21425-21442.

Table 1: Summary of the model experiments performed for this study. The period of the QBO is calculated at 30 hPa.

	Injection burden [Tg-SO_2]	Injection altitude [km]	Aerosol stratospheric burden [Tg-S]	QBO Period (std. deviation) [months]
control	-	-	-	25.1 (4.0)
$G_{2..5}^{16\text{-}25km}$	2.5	16 – 25	1.5	26.8 (10.1)
$G_{2.5}^{22\text{-}25km}$	2.5	22 – 25	2.1	29.0 (5.4)
$G_{5}^{16\text{-}25km}$	5	16 – 25	3.1	50.8 (2.2)
$G_{5}^{22\text{-}25km}$	5	22 – 25	4.7	-

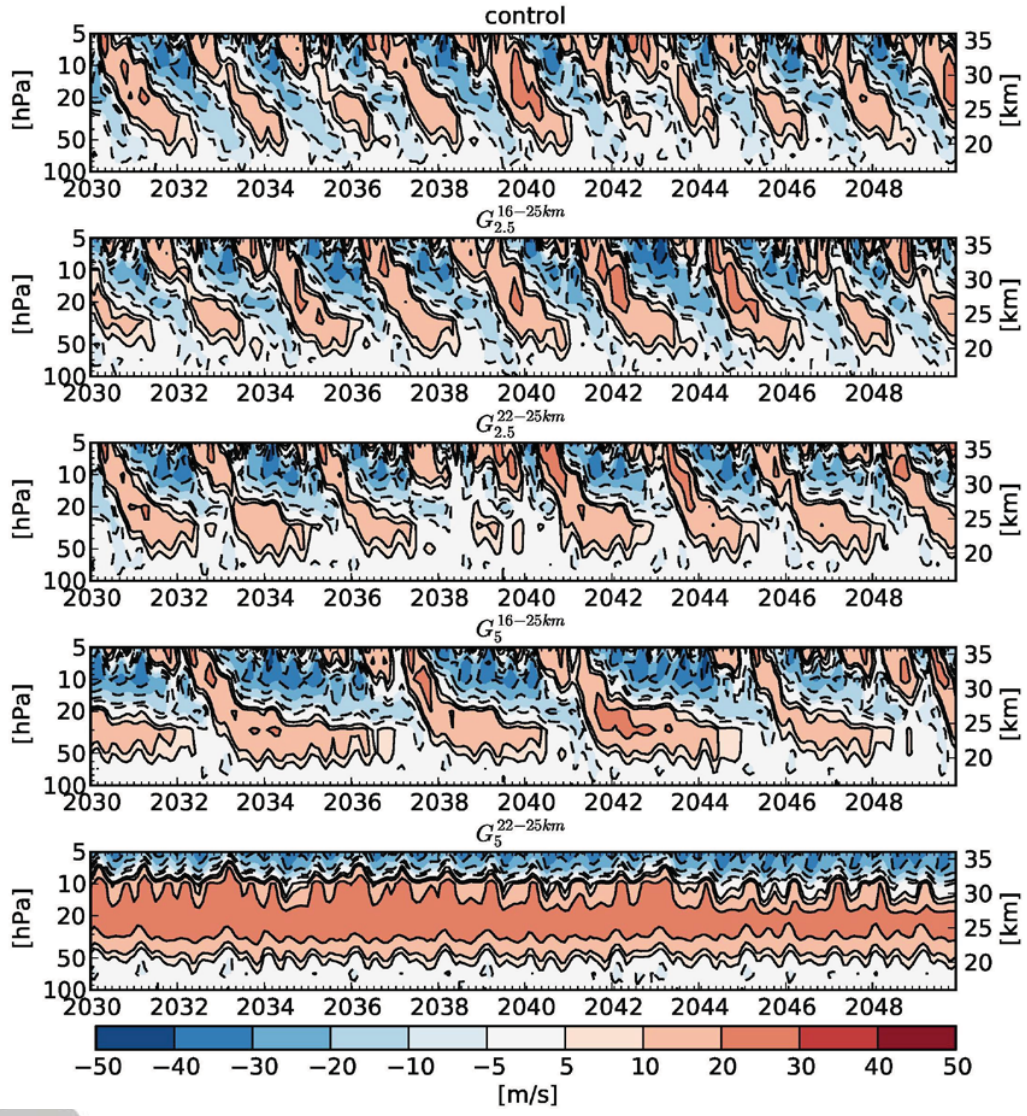

Fig.1: Vertical profiles of the zonal wind, zonally averaged between 2˚S and 2˚N in (from top to bottom) control run, $G_{2.5}^{16\text{-}25km}$, $G_{2.5}^{22\text{-}25km}$, $G_{5}^{16\text{-}25km}$, $G_{5}^{22\text{-}25km}$.

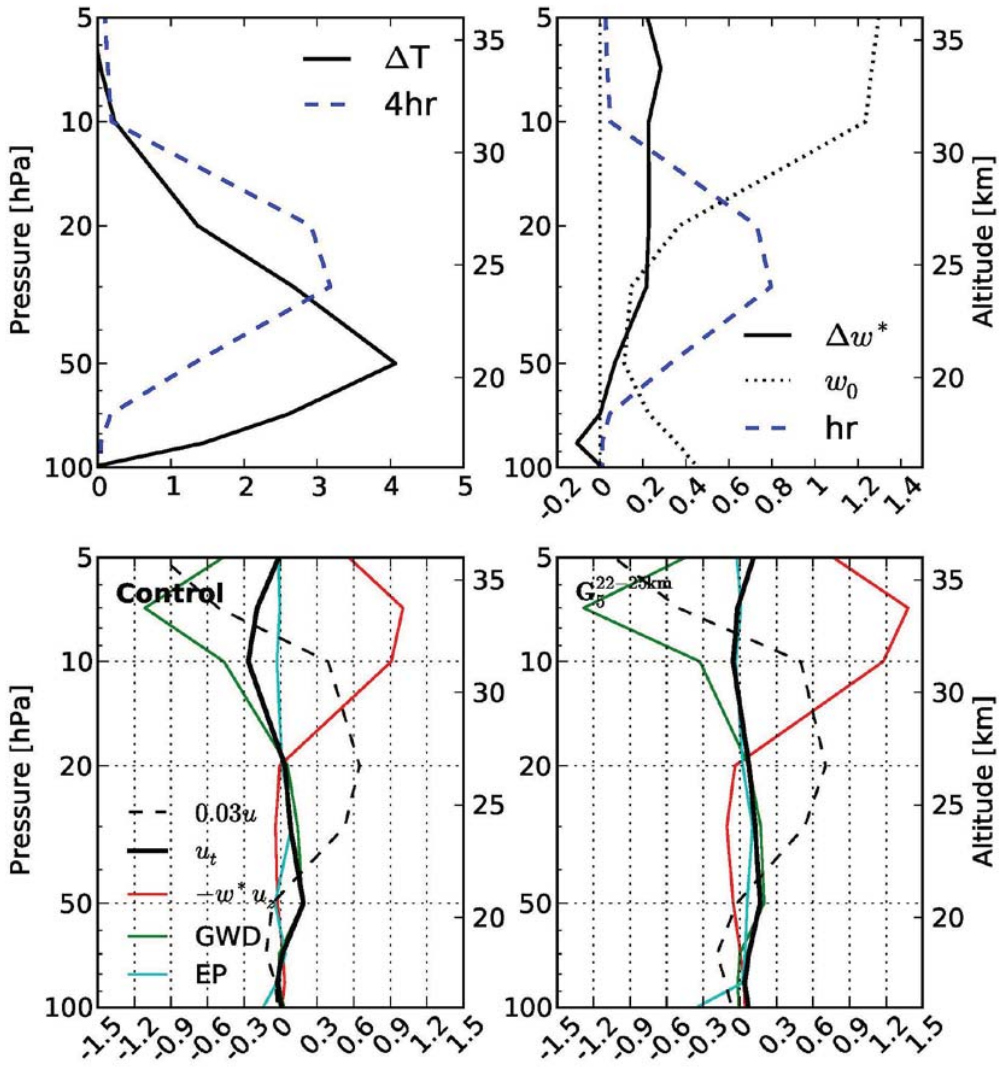

Fig.2: Upper panels: Vertical profiles of the zonal mean (2°S -2°N) anomaly of the temperature anomaly (upper left, in K) and residual vertical velocity (upper right, in mm/s). The anomalies are calculated between the two months of the control and $G_5^{22\text{-}25km}$ when the *u* wind profiles are the most similar. The dashed blue line shows the aerosol heating rates in K/day in $G_5^{22\text{-}25km}$ (note the scaling factor in the upper left figure). The dotted black line in the upper right panel shows $\overline{w}^*$ in the control simulation. Lower panels: Vertical profiles of the forcing terms (in m s^{-1} day^{-1}) that drive the QBO in the control (left) and $G_5^{22\text{-}25km}$ (right) simulations during the months considered in the upper panels. Shown are the 2°S-2°N zonal means of *u* wind in m/s multiplied by a factor 0.03 (dashed black), the time derivative of *u* (solid black), the advection of the mean flow (red), the parameterized gravity wave drag (green) and the divergence of the Eliassen-Palm flux (blue).

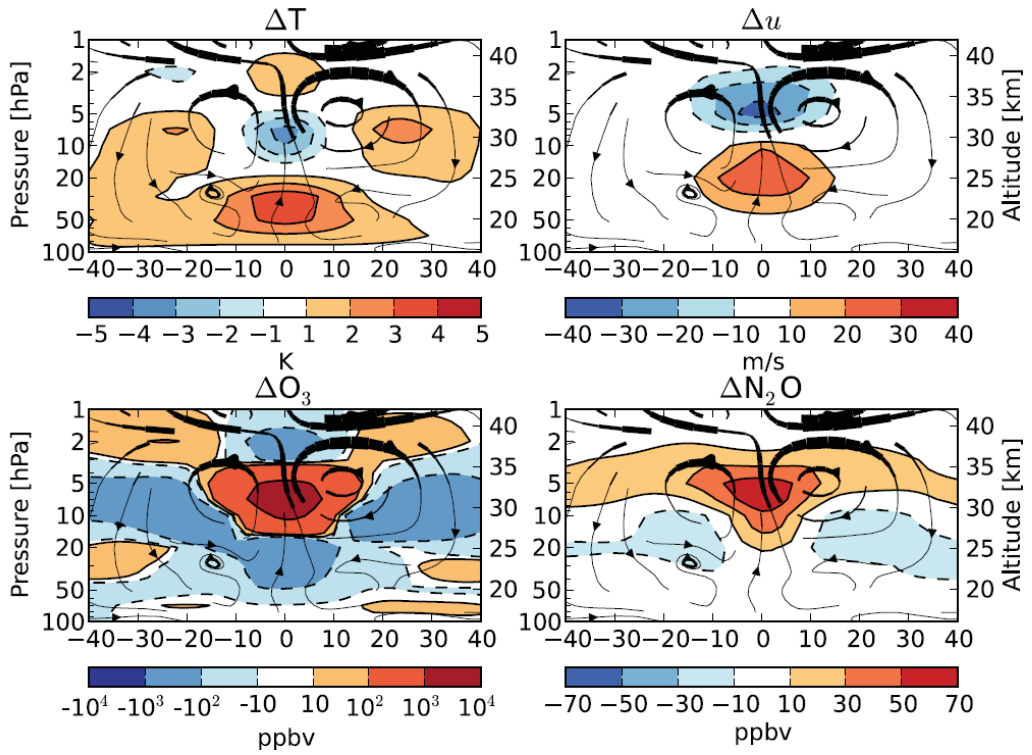

Fig.3: Vertical profiles of the zonal mean anomalies of temperature, zonal wind *u*, ozone and N_2O concentrations in $G_5^{22\text{-}25km}$ with respect to the control simulation. The streamlines show the anomaly of the residual circulation. The anomalies are calculated over the whole 2030-2050 period. The thickness of the streamlines is proportional to the change of speed.